NANO LETTERS

2007
Vol. 7, No. 12
3618−3622

# Direct Observation of Mode Selective Electron–Phonon Coupling in Suspended Carbon Nanotubes

**Adam W. Bushmaker,[†] Vikram V. Deshpande,[‡] Marc W. Bockrath,[‡] and Stephen B. Cronin*[,†]**

*Department of Electrical Engineering, University of Southern California, Los Angeles, California 90089, and Applied Physics, California Institute of Technology, Pasadena, California 91125*

*Received July 27, 2007; Revised Manuscript Received October 19, 2007*

**ABSTRACT**

**Raman spectra of individual pristine suspended single-walled carbon nanotubes are observed under high electrical bias. The LO and TO modes of the *G* band behave differently with respect to voltage bias, indicating preferential electron–phonon coupling and nonequilibrium phonon populations, which cause negative differential conductance in suspended devices. By correlating the electron resistivity to the optically measured phonon population, the data are fit using a Landauer model to determine the key scattering parameters.**

Electron−phonon coupling in carbon nanotubes has been studied by many research groups.[1−7] In metallic carbon nanotubes (m-CNTs), conduction electrons have been predicted to couple strongly to the Γ-point longitudinal optical (LO) phonons and to the $2k_F$-point transverse optical (TO) phonons.[1−6] The *G* band Raman spectra of m-CNTs and semiconducting CNTs (s-CNT) are qualitatively different because of this strong electron−phonon coupling.[8] In metallic nanotubes, the lower-frequency component of the *G* band ($G_-$) exhibits a broad Breit−Wigner−Fano (BWF) line shape and is significantly downshifted in frequency with respect to its counterpart in semiconducting nanotubes.[9] Recent experiments have shown that this phonon softening can be removed by shifting the Fermi energy of m-CNTs with an applied gate voltage or chemical doping, which modulates this coupling and results in an upshift of the $G_-$ band frequency.[10−12] Density functional theory calculations have shown that the assignment of the upper and lower frequency components of the *G* band Raman modes, $G_+$ and $G_-$, to the LO and TO Γ-point phonon modes may be reversed in m-SWNTs and s-SWNTs.[13] This is thought to be caused by the strong downshifting of the LO mode due to the Kohn anomaly, also referred to as a Peierls-like distortion phenomenon.[6,14] Other experiments have shown that this downshift may be caused by internanotube bundling effects.[15]

Negative differential conductance (NDC) has been observed by several research groups at high-voltage bias in suspended nanotubes and is understood on the basis of electrons coupling strongly to Γ-point and $2k_F$-point optical phonons (OPs).[16−18] At high-voltage bias, the electrons emit OPs, causing increased scattering from absorption of those OPs, and an increase in resistance. In the experiment reported here, we simultaneously observe the OP populations and nanotube resistance and are able to correlate the electron scattering length to phonon population.

When CNTs are heated, the *G* band downshifts in frequency,[19−26] broadens,[27] and decreases in intensity[19,21] due to thermal expansion, which weakens the bonds. In thermal equilibrium, both the LO and TO phonons downshift together. We observe preferential downshifting of only one of the OPs at high currents, indicating strong coupling of electrons to only one band and a nonequilibrium phonon population.

Preferential e-ph coupling and coherent phonon generation was first reported in Ruby in 1961[28] and was followed by other reports describing the phenomenon in GaAs and other semiconductor crystals.[29−31] More recent work analyzed selective amplification and emission of OPs in electron transport experiments[32] and a full quantum treatment of THz phonon laser design.[33] This observation of selective e-ph coupling in carbon nanotubes supports the possibility of using carbon nanotubes as a source of coherent phonons as suggested elsewhere.[18]

Suspended SWNTs were grown using chemical vapor deposition on Pt electrodes prepared with islands of lithographically patterned catalyst. Out of 40 devices per chip, typically only a few have just one SWNT bridging the

* Corresponding author. Phone: 213-740-8787. E-mail: scronin@usc.edu.
[†] University of Southern California.
[‡] California Institute of Technology.

10.1021/nl071840f CCC: $37.00 
**Published on Web 11/20/2007**

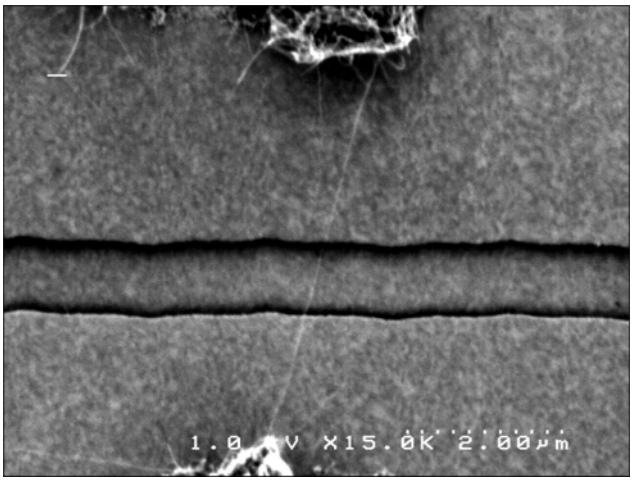


**Figure 1.** SEM image of a suspended carbon nanotube grown on top of Pt electrodes.

contacts of the device. The trench width for the devices range from 0.5 to 2 $\mu$m. Figure 1 shows one such device fabricated in this study. Raman spectra were measured in a Renishaw InVia spectrometer with a 785 nm Ti-Sapphire laser. An Ithaco current preamplifier was used to measure the current passed through the nanotube.

Sample fabrication proceeds as follows. A trench is first made between two Pt electrodes on a degenerately doped Si substrate by one of two methods.[34,35] In the first method, Pt electrodes are patterned by lithography on a Si substrate capped with 300 nm of $SiO_2$, which is then wet-etched in HF using the Pt electrodes as an etch mask. In the second method, the Si substrate is capped with 500 nm of $SiO_2$ and 50 nm of $Si_3N_4$. The nitride is then dry-etched in a $CF_4$ plasma to form the trench, the underlying oxide is wet-etched, and the Pt contacts are then patterned. Islands of Fe−Mo catalyst salts in an alumina matrix are then defined on top of the contacts in lithographically defined areas.[36] Nanotube growth is carried out by flowing a mixture of methane (0.5 SLM) and hydrogen (0.7 SLM) over the wafer for 5 min at 800 °C. Devices that show negative differential conductance at high bias (1−2 V) with a maximum current of $\sim 10/L$ $\mu$A (where $L$ is in $\mu$m) correspond to individual suspended single-walled nanotubes and are selected for further study.[16]

Figure 2 shows the $G$ band Raman modes of a nanotube device under large voltage biases. The band gap of this nanotube was determined to be ~60 meV from the current-gate voltage dependence. The $G_+$ band is observed to downshift by more than 26 $cm^{-1}$, while the $G_-$ on average does not change by more than 1 $cm^{-1}$. There is a clear crossing that occurs at ~1.0 V above which the $G_-$ band becomes higher in frequency than the $G_+$ band. The linewidths of the $G_+$ and $G_-$ bands in the nanotube of Figure 2 also vary with the applied bias voltage. Here the $G_+$ band broadens while the $G_-$ band remains largely unchanged. Finally, the intensity of the $G_+$ band decreases monotonically with bias voltage, while the $G_-$ band remains constant. This behavior suggests preferential heating of the $G_+$ phonon mode, because the $G$ band Raman spectra are known to downshift, broaden, and diminish in intensity with increasing temperature.[19−27] The integrated areas of both the $G_+$ and the $G_-$ Raman peaks remain constant, indicating that there is no change in the resonance condition of this nanotube with applied bias. Preferential heating of the $G_+$ phonon was observed in 4 out of 15 devices measured in this study, including one semiconducting device. Because the unbiased $G_-$ band exhibits a broad, downshifted BWF line shape, we assign it to the LO phonon mode, and we assign the $G_+$ to the TO phonon mode.

Figure 3 shows the $G$ band Raman modes of another nanotube under large voltage biases. NDC can be clearly seen above 1.2 V in the current−voltage ($I-V_{bias}$) characteristics of this device, as shown in the inset of Figure 3. Here, the voltage dependence of the $G_+$ and $G_-$ bands are reversed from those shown in Figure 2. Over the range of applied bias voltage, the $G_-$ band is observed to downshift by 15 $cm^{-1}$, while the $G_+$ band does not change by more than 1 $cm^{-1}$. Furthermore, the line width of the $G_-$ band increases significantly with bias voltage and drops in intensity, while the $G_+$ band remains of constant width and intensity. Contrary to Figure 2, this data exhibits preferential heating of the $G_-$ band, which we again assign to the LO Γ-point phonon mode. This case is rare and was only observed in one out of fifteen nanotubes measured in this study. Again, the integrated areas of both the $G_+$ and $G_-$ peaks remain constant, indicating that there is no change in the resonance condition. The broadening of the $G_+$ feature

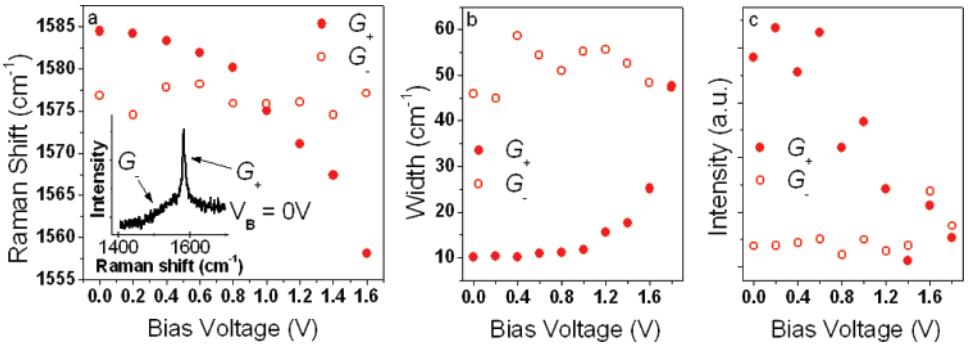


**Figure 2.** $G$ band Raman spectral data versus bias voltage. $G$ band Raman (a) shift, (b) width, and (c) intensity. The inset shows the Raman spectra at zero bias voltage.

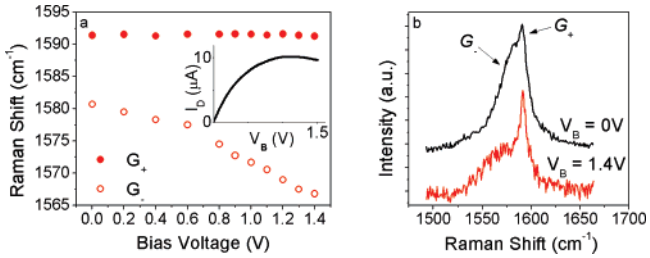


**Figure 3.** (a) The *G* band Raman shift versus bias voltage, with the $I-V_{bias}$ inset exhibiting NDC. (b) Raman spectra taken at $V_{bias} = 0$ and 1.4 V.

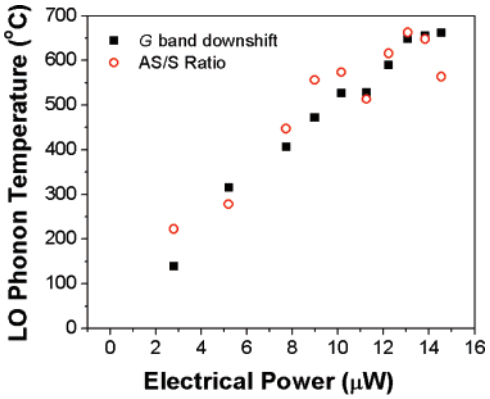


**Figure 4.** Optical phonon temperature vs electrical power. Temperature is measured for the device in Figure 3 by AS/S Raman spectroscopy and by *G* band downshift.

is consistent with thermal broadening in SWNTs as reported by Jorio et al.[27] Both nanotubes shown in Figures 2 and 3 are metallic, and all changes in the Raman spectra are reversible.

A weak radial breathing mode (RBM) was observed in the Raman spectra of this nanotube at 146.5 cm$^{-1}$, which corresponds to a nanotube diameter of 1.70 nm by the relation $\omega_{RBM} = 204/d_t + 27$.[37] The strongly enhanced Raman intensities from suspending the carbon nanotubes off the substrate[38] make it possible to observe RBMs with the incident laser off resonance. The weak RBM observed for this nanotube implies an off-resonance condition, which creates significant uncertainty in the transition energy $E_{ii}$ and hence the chirality assignment of this nanotube. The peak current density of this nanotube can be obtained by dividing the peak current (10 $\mu$A) by the cross-sectional area of the nanotube ($1.9 \times 10^{-18}$ m$^2$), obtained by multiplying the circumference of the nanotube with the thickness of graphene (0.355 nm). This results in a peak current density of $5.3 \times 10^8$ A/cm$^2$.

The behaviors shown in Figures 2 and 3 can be explained by the previous theoretical work of Piscanec et al.,[13] which describes the strong electron−phonon coupling of the Kohn anomalies (KA) in metallic carbon nanotubes. One KA occurs at zero momentum (Γ-point) in the LO phonon band and gives the $G_-$ band in metallic nanotubes its downshifted and broadened BWF line shape.[39] Another KA occurs at a finite phonon momentum $q = 4\pi/3T$ ($2k_F$-point) in the TO phonon branch, where $T$ is the length of the unit cell in the nanotube. These two KAs provide the primary source of electron−phonon scattering in pristine m-CNTs at high-bias voltages.

It is surprising that the narrow $G_+$ band (TO band) in Figure 2 is so strongly coupled to the electrons, while the broad $G_-$ band (LO band) remains unchanged with applied bias voltage. We can explain this by considering that the energy of the $2k_F$-point phonons associated with the TO KA is significantly lower than the energy of the Γ-point phonons of the LO KA. This results in a lower threshold energy for TO phonon emission in electron transport. Thus the electrons are scattered by emitting TO phonons before ever attaining enough energy to emit LO phonons, which results in heating of only the TO phonon band. This, together with the fact that the electron−phonon coupling for the $2k_F$-point KA is two times stronger than that of the Γ-point KA,[13] explains why the $G_+$ band (TO) is observed to be strongly heated for nanotubes of the type shown in Figure 2. While the finite momentum phonons cannot be observed directly in first-order Raman spectra, the modes in each phonon branch are expected to equilibrate thermally. The orthogonality of the LO and TO phonon bands enables them to remain in a state of extreme nonequilibrium and exhibit preferential heating.

The seemingly contradictory results of Figure 3 in which only the $G_-$ band (LO) downshifts with applied bias voltage can be understood on the basis of a particular chirality, where

$$R = \frac{GCD(n,m)}{GCD(2n+m,\, 2m+n)} = 1$$

which only occurs for slightly less than 1/3 of all metallic nanotubes. In fact, this behavior was only observed in one out of fifteen nanotubes measured in this study, which is consistent with the rarity of this chirality. In this case, the Raman active TO phonon branch does not exhibit a KA,[13] and heating by hot electrons is only observed in the LO phonon band.

The high temperatures reached under large voltage biases were corroborated by anti-Stokes (AS) Raman spectroscopy. A *G* band AS peak was observed at biases above 0.4 V on the device shown in Figure 3. The ratio of the AS (absorbed phonons) to the Stokes (emitted phonons) Raman intensity is given by the Maxwell−Boltzmann factor $\exp(-E_{ph}/k_BT)$, where $E_{ph}$ is the phonon energy (195 meV), $k_B$ is Boltzmann's constant, and $T$ is the temperature in Kelvin. Figure 4 shows the temperature as determined from the AS/S ratio plotted as a function of electrical power. The temperature shows a linear dependence on electrical power that reaches ~700 °C at high bias. At higher voltages, the nanotube was destroyed. This temperature is consistent with the work of Cataldo, who measured the burnout threshold of carbon nanotubes in air to be ~800 °C.[40] The optical phonon temperature was also determined independently from the downshift of the $G_-$ band by the relation $\omega_{G,LO}(T) = -3.5 \times 10^{-5} \cdot T^2 - 6.5 \times 10^{-3} \cdot T + 1581.5$, which was measured on one of our devices in a temperature-controlled stage. This data is also plotted in Figure 4 and is in good agreement with the AS/S ratio data. We would like to point out that,

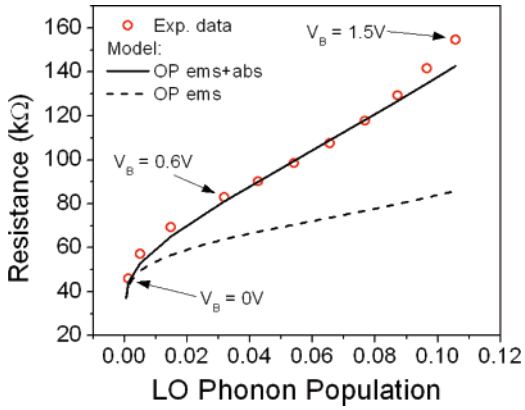


**Figure 5.** Electrical resistance plotted as a function of phonon population. The phonon population is fit from the measured data in Figure 4 for the device in Figure 3. The two models shown are for LO scattering through emission plus nonequilibrium OP absorption and through OP emission alone.

while the AS spectra of the LO mode yields a temperature of ~700 °C, the TO mode was not observed in the AS spectra. This, together with the lack of change in the TO Stokes Raman frequency, indicates that the population of the TO phonon remains close to room temperature. These data show that the coupling between the two OP polarizations (LO and TO) is very weak and that they can exist in a state of extreme nonequilibrium.

By measuring electrical resistivity and optical phonon population simultaneously, we gain new information about the phonon-scattering mechanism responsible for the observed NDC[16,17] as suggested by Lazzeri.[18] Figure 5 shows the electrical resistance plotted as a function of LO phonon population $N_{op}(T_{op})$, which is fitted from the experimental data in Figure 4. We can understand this data using the Landauer model developed by Pop,[16,41] Mann,[17] Park,[42] Yao,[43] and others[18,44] in which the nanotube resistance is expressed as

$$R(V,T) = R_c + \frac{h}{4q^2}\frac{L + \lambda_{eff}(V,T)}{\lambda_{eff}(V,T)} \quad (1)$$

where $R_c$ is the contact resistance, $L$ is the nanotube length, and $\lambda_{eff} = (\lambda_{ac}^{-1} + \lambda_{op,ems}^{-1} + \lambda_{op,abs}^{-1})^{-1}$ is the bias and temperature-dependent electron mean-free path.[16,17] The acoustic-scattering length is given by $\lambda_{ac} = \lambda_{ac}^{RT}$ (300 K/$T_{ac}$)$^{-1}$. The acoustic phonon temperature is $T_{ac} = (T_{op} + \alpha T_{sample})/(1 + \alpha)$, where the nonequilibrium phonon coefficient $\alpha$ is taken as 2.3 from Mann et al.[17] and the optical phonon temperature $T_{op}$ is measured by Raman spectroscopy. The optical phonon-scattering length for emitted phonons is given by

$$\lambda_{op,ems} = \frac{E_{ph}L}{qV} + \lambda_{op}^{min}\left(\frac{1 + N_{op}(300\ K)}{1 + N_{op}(T_{op})}\right) \quad (2)$$

and for absorbed phonons by

$$\lambda_{op,abs} = \lambda_{op}^{min}\left(\frac{1 + N_{op}(300\ K)}{N_{op}(T_{op})}\right) \quad (3)$$

In these equations, $E_{ph}$ is the OP energy, and $\lambda_{op}^{min}$ is the scattering length for electron scattering from OP emission in the nanotube after the electron has accelerated to high energy $\geq E_{ph}$. Low-energy electrons may scatter with this length scale from absorption of thermally populated OPs as well, as described by eq 3. In addition to the constant contact resistance $R_c$, this model has one fitting parameter, $\lambda_{op}^{min}$. An approximate value of $\lambda_{ac}^{RT}$= 2400 nm was used in the fit in accordance with previous work,[42] and the fitted value for $\lambda_{op}^{min}$ was generally found to be insensitive to the value of $\lambda_{ac}^{RT}$.

The solid and dashed lines in Figure 5 correspond to fits of our data using this model with OP emission and absorption and with OP emission alone, respectively, with $\lambda_{op}^{min}$ = 26 nm. This value is consistent with those reported previously in the literature.[42,45] The model including OP emission and absorption is in good agreement with the experimental results for phonon populations below 0.09. The failure of the model without OP absorption indicates the important role that the nonequilibrium optical phonon population plays in the electron transport of suspended SWNTs. At larger phonon populations, corrections to the model are needed to account for the nonuniformity of the temperature along the length of the nanotube, as shown previously in finite element thermal analysis calculations.[17]

We have performed a systematic study measuring the optical and high-bias electronic properties of five suspended nanotubes that exhibited preferential downshifting of the $G_+$ or $G_-$ band. This data has been fit to the model described above, and their results are listed in Table 1. Table 1 lists the metallic/semiconducting nature and band gap of the nanotubes, as determined from the electron transport data. The Raman feature that is preferentially downshifted with bias voltage is also indicated in Table 1. The diameter is indicated for nanotubes that exhibited a RBM in their spectra. Despite the very different results observed in their optical spectra, we find little variation in the optical phonon-scattering parameter $\lambda_{op}^{min}$ among m-SWNTs.

Ten out of the 15 nanotubes measured in this study did not exhibit preferential downshifting of the $G_+$ or $G_-$ bands and were not included in Table 1. In 5 of these 10 nanotubes, the relative intensity of the $G_+/G_-$ bands was so great that a clear resolution of both peak positions was not possible, and hence it was not possible to observe whether preferential heating occurred. The $G_+/G_-$ intensity ratio has been theoretically predicted and experimentally shown to be a function of chiral angle.[46,47] We attribute the behavior of these five nanotubes to the extreme cases of large and small chiral angles. In the remaining five nanotubes not shown in Table 1, both the $G_+$ and the $G_-$ bands downshifted when heated with electrical current. This is attributed to anomalous phonon−phonon anharmonic coupling and further indicates the high purity of the pristine nanotube samples that did exhibit strong selective coupling and extreme nonequilibrium phonon populations.

**Table 1.** Summary of Electron and Phonon Parameters of Five Suspended Nanotubes

| sample | length ($\mu$m) | M/SC | downshift | $d_t$ (nm) | $\lambda_{op}^{min}$ (nm) |
|---|---|---|---|---|---|
| 1 | 0.5 | M | $G_+$ | | 18 |
| 2 | 2 | M | $G_-$ | 1.7 | 26 |
| 3 | 1 | M | $G_+$ | | 35 |
| 4 | 2 | SC | $G_+$ | 2.0 | 9 |
| 5 | 0.5 | M | $G_+$ | | 28 |

In conclusion, we observe preferential electron−phonon coupling of the *G* band Raman modes in carbon nanotubes under high-voltage bias. This preferential coupling is caused by the differences between the two Kohn anomalies in the TO and LO phonons bands. Surprisingly, in most metallic nanotubes, the narrow $G_+$ band (TO band) is strongly heated by electron−phonon scattering at high biases. Because of the preferential electron−phonon coupling, high-voltage biases produce a nonequilibrium phonon population, as observed by AS Raman spectroscopy. By correlating the electron resistivity to the phonon population, measured by Raman spectroscopy, we determine the high-energy electron−OP scattering length $\lambda_{op}^{min}$ in m-SWNTs to be $\sim$ 30 nm.

**Acknowledgment.** This research was supported in part by DOE Award No. DE-FG02-07ER46376, the James H. Zumberge Fund, the Powell Foundation, and the National Science Foundation Graduate Research Fellowship Program.

## References

(1) Samsonidze, G. G.; Barros, E. B.; Saito, R.; Jiang, J.; Dresselhaus, G.; Dresselhaus, M. S. *Phys. Rev. B.* **2007**, *75* (15), 155420−8.
(2) Lazzeri, M.; Mauri, F. *Phys. Rev. B* **2006**, *73* (16), 165419.
(3) Dubay, O.; Kresse, G. *Phys. Rev. B* **2003**, *67* (3), 035401.
(4) Caudal, N.; Saitta, A. M.; Lazzeri, M.; Mauri, F. *Phys. Rev. B.* **2007**, *75* (11), 115423−11.
(5) Lazzeri, M.; Piscanec, S.; Mauri, F.; Ferrari, A. C.; Robertson, J. *Phys. Rev. B* **2006**, *73* (15), 155426.
(6) Dubay, O.; Kresse, G.; Kuzmany, H. *Phys. Rev. Lett* **2002**, *88* (23), 235506.
(7) Capaz, R. B.; Spataru, C. D.; Tangney, P.; Cohen, M. L.; Louie, S. G. *Phys. Rev. Lett.* **2005**, *94* (3), 36801.
(8) Dresselhaus, M. S.; Dresselhaus, G.; Jorio, A.; Souza Filho, A. G.; Saito, R. *Carbon* **2002**, *40* (12), 2043−2061.
(9) Dresselhaus, M. S.; Dresselhaus, G.; Saito, R.; Jorio, A. *Phys. Rep.* **2005**, *409* (2), 47−99.
(10) Kavan, L.; Rapta, P.; Dunsch, L.; Bronikowski, M. J.; Willis, P.; Smalley, R. E. *J. Phys. Chem. B* **2001**, *105* (44), 10764−10771.
(11) Rafailov, P. M.; Maultzsch, J.; Thomsen, C.; Kataura, H. *Phys. Rev. B* **2005**, *72* (4), 45411.
(12) Cronin, S. B.; Barnett, R.; Tinkam, M.; Chou, S. G.; Rabin, O.; Dresselhaus, M. S.; Swan, A. K.; Ünlü, M. S.; Goldber, B. B. *App. Phys. Lett.* **2004**, *84* (12), 2052.
(13) Piscanec, S.; Lazzeri, M.; Robertson, J.; Ferrari, A. C.; Mauri, F. *Phys. Rev. B* **2007**, *75* (3), 35427.
(14) Reich, S.; Thomsen, C.; Maultzsch, J. *Carbon Nanotubes: Basic Concepts and Physical Properties*; Wiley-VCH: New York, 2004.
(15) Kumar, R.; Cronin, S. B. *Phys. Rev. B* **2007**, *75* (15), 155421−4.
(16) Pop, E.; Mann, D.; Cao, J.; Wang, Q.; Goodson, K.; Dai, H. *Phys. Rev. Lett.* **2005**, *95* (15), 155505.
(17) Mann, D.; Pop, E.; Cao, J.; Wang, Q.; Goodson, K.; Dai, H. *J. Phys. Chem. B* **2006**, *110* (4), 1502−1505.
(18) Lazzeri, M.; Piscanec, S.; Mauri, F.; Ferrari, A. C.; Robertson, J. *Phys. Rev. Lett.* **2005**, *95*, 236802.
(19) Atashbar, M. Z.; Singamaneni, S. *App. Phys. Lett.* **2005**, *86* (12), 123112−3.
(20) Bassil, A.; Puech, P.; Tubery, L.; Bacsa, W.; Flahaut, E. *Appl. Phys. Lett.* **2006**, *88* (17), 173113−3.
(21) Chiashi, S.; Murakami, Y.; Miyauchi, Y.; Maruyama, S. *Chem. Phys. Lett.* **2004**, *386* (1−3), 89−94.
(22) Ci, L.; Zhou, Z.; Song, L.; Yan, X.; Liu, D.; Yuan, H.; Gao, Y.; Wang, J.; Liu, L.; Zhou, W.; Wang, G.; Xie, S. *App. Phys. Lett.* **2003**, *82* (18), 3098−3100.
(23) Huang, F.; Yue, K. T.; Tan, P.; Zhang, S.-L.; Shi, Z.; Zhou, X.; Gu, Z. *J. Appl. Phys.* **1998**, *84* (7), 4022−4024.
(24) Huong, P. V.; Cavagnat, R.; Ajayan, P. M.; Stephan, O. *Phys. Rev. B* **1995**, *51* (15), 10048.
(25) Li, H. D.; Yue, K. T.; Lian, Z. L.; Zhan, Y.; Zhou, L. X.; Zhang, S. L.; Shi, Z. J.; Gu, Z. N.; Liu, B. B.; Yang, R. S.; Yang, H. B.; Zou, G. T.; Zhang, Y.; Iijima, S. *Appl. Phys. Lett.* **2000**, *76* (15), 2053−2055.
(26) Raravikar, N. R.; Keblinski, P.; Rao, A. M.; Dresselhaus, M. S.; Schadler, L. S.; Ajayan, P. M. *Phys. Rev. B* **2002**, *66* (23), 235424.
(27) Jorio, A.; Fantini, C.; Dantas, M. S. S.; Pimenta, M. A.; Souza Filho, A. G.; Samsonidze, G. G.; Brar, V. W.; Dresselhaus, G.; Dresselhaus, M. S.; Swan, A. K.; Ünlü, M. S.; Goldberg, B. B.; Saito, R. *Phys. Rev. B* **2002**, *66* (11), 115411.
(28) Tucker, E. B. *Phys. Rev. Lett.* **1961**, *6* (10), 547.
(29) Nahory, R. E. *Phys. Rev. Lett.* **1969**, *178* (3), 1293.
(30) Shaw, R. W. *Phys. Rev. B* **1971**, *3* (10), 3283.
(31) Merlin, R. *Solid State Commun.* **1997**, *102* (2−3), 207−220.
(32) Rodrigues, C. G.; Vasconcellos, A. R.; Luzzi, R. *Solid State Commun.* **2006**, *140* (3−4), 135−140.
(33) Camps, I.; Makler, S. S.; Pastawski, H. M.; Foa Torres, L. E. F. *Phys. Rev. B* **2001**, *64* (12), 125311.
(34) Cao, J.; Wang, Q.; Wang, D.; Dai, H. *Nanotube Devices* **2005**, *1* (1), 138−141.
(35) Qi, P.; Vermesh, O.; Grecu, M.; Javey, A.; Wang, Q.; Dai, H.; Peng, S.; Cho, K. J. *Nano Lett.* **2003**, *3* (3), 347−351.
(36) Kong, J.; Soh, H. T.; Cassell, A. M.; Quate, C. F.; Dai, H. *Nature* **1998**, *395* (6705), 878−881.
(37) Meyer, J. C.; Paillet, M.; Michel, T.; Moreac, A.; Neumann, A.; Duesberg, G. S.; Roth, S.; Sauvajol, J.-L. *Phys. Rev. Lett.* **2005**, *95* (21), 217401−4.
(38) Zhang, Y.; Zhang, J.; Son, H.; Kong, J.; Liu, Z. *J. Am. Chem. Soc.* **2005**, *127* (49), 17156−17157.
(39) Brown, S. D. M.; Jorio, A.; Corio, P.; Dresselhaus, M. S.; Dresselhaus, G.; Saito, R.; Kneipp, K. *Phys. Revi. B* **2001**, *63* (15), 155414.
(40) Cataldo, F. *Fullerenes, Nanotubes, Carbon Nanostruct.* **2002**, *10* (4), 293−311.
(41) Pop, E.; Mann, D. A.; Goodson, K. E.; Dai, H. *J. Appl. Phys.* **2007**, *101* (9), 093710−10.
(42) Park, J. Y.; Rosenblatt, S.; Yaish, Y.; Sazonova, V.; Ustunel, H.; Braig, S.; Arias, T. A.; Brouwer, P. W.; McEuen, P. L. *Nano Lett.* **2003**, *4* (3), 517.
(43) Yao, Z.; Kane, C. L.; Dekker, C. *Phys. Rev. Lett.* **2000**, *84* (13), 2941.
(44) Kane, C. L.; Mele, E. J.; Lee, R. S.; Fischer, J. E.; Petit, P.; Dai, H.; Thess, A.; Smalley, R. E.; Verschueren, A. R. M.; Tans, S. J. *Europhys. Lett.* **1998**, *41* (6), 683−688.
(45) Javey, A.; Guo, J.; Paulsson, M.; Wang, Q.; Mann, D.; Lundstrom, M.; Dai, H. *Phys. Rev. Lett.* **2004**, *92* (10), 106804−4.
(46) Saito, R.; Jorio, A.; Hafner, J. H.; Lieber, C. M.; Hunter, M.; McClure, T.; Dresselhaus, G.; Dresselhaus, M. S. *Phys. Rev. B* **2001**, *64* (8), 085312.
(47) Wu, Y.; Maultzsch, J.; Knoesel, E.; Chandra, B.; Huang, M.; Sfeir, M. Y.; Brus, L. E.; Hone, J.; Heinz, T. F. *Phys. Rev. Lett.* **2007**, *99* (2), 027402−4.

NL071840F